Nuclear Engineering and Technology xxx (xxxx) xxx

Contents lists available at ScienceDirect

Nuclear Engineering and Technology

journal homepage: www.elsevier.com/locate/net

Original article

Gamma/neutron classification with SiPM CLYC detectors using frequency-domain analysis for embedded real-time applications

Iván René Morales [a,b,*], Maria Liz Crespo [a], Mladen Bogovac [c], Andres Cicuttin [a], Kalliopi Kanaki [c], Sergio Carrato [b]

[a] Multidisciplinary Laboratory (MLab), STI Unit, The Abdus Salam International Centre for Theoretical Physics (ICTP), Strada Costiera, 11, Trieste, 34151, TS, Italy

[b] Dipartimento di Ingegneria e Architettura (DIA), Università degli Studi di Trieste (UNITS), Piazzale Europa, 1, Trieste, 34127, TS, Italy

[c] Nuclear Science and Instrumentation Laboratory, Physics Section, Division of Physical & Chemical Sciences, Department of Nuclear Sciences & Applications, Vienna International Centre, Vienna, A-1400, Austria

ARTICLE INFO

Keywords:
CLYC
Gamma/neutron classification
SiPM
FFT
Embedded systems
FPGA
Gamma/neutron discrimination

ABSTRACT

A method for gamma/neutron event classification based on frequency-domain analysis for mixed radiation environments is proposed. In contrast to the traditional charge comparison method for pulse-shape discrimination, which requires baseline removal and pulse alignment, our method does not need any preprocessing of the digitized data, apart from removing saturated traces in sporadic pile-up scenarios. It also features the identification of neutron events in the detector's full energy range with a single device, from thermal neutrons to fast neutrons, including low-energy pulses, and still provides a superior figure-of-merit for classification.

The proposed frequency-domain analysis consists of computing the fast Fourier transform of a triggered trace and integrating it through a simplified version of the transform magnitude components that distinguish the neutron features from those of the gamma photons. Owing to this simplification, the proposed method may be easily ported to a real-time embedded deployment based on Field-Programmable Gate Arrays or Digital Signal Processors. We target an off-the-shelf detector based on a small CLYC (Cs2LiYCl6:Ce) crystal coupled to a silicon photomultiplier with an integrated bias and preamplifier, aiming at lightweight embedded mixed radiation monitors and dosimeter applications.

1. Introduction

One of the most efficient options for thermal neutron (n_{th}) detectors today relies on the ^{3}He isotope, taking advantage of its large neutron capture cross section and low sensitivity to gamma (γ) events. However, because of the shortage of such material, alternatives have been developed to overcome this problem [1–3]. The CLYC (Cs2LiYCl6:Ce) crystal is an excellent example of a substitute n_{th} detector [4–9]. This crystal also exhibits similar γ efficiency and exceeds the energy resolution compared to conventional NaI(Tl) scintillators [10,11]. More recently, the CLYC capability for fast neutron (n_f) detection and spectroscopy was discovered, turning the crystal into a triple-purpose material: thermal neutron detection, gamma spectroscopy, and fast neutron spectroscopy [11–13].

In this paper, we propose a method to exploit the γ/n classification features of a small CLYC crystal coupled to a silicon photomultiplier (SiPM) sensor array with an integrated preamplifier and bias power supply. These types of integrated detectors require less complex electronics, weigh less, and occupy less volume than traditional photomultiplier (PMT) solutions [14,15]. Integrated detection systems like these are useful in applications such as remote mixed radiation monitoring [16], including fusion reactor diagnostics [17], space exploration field dosimetry [18], among others.

Using a simplified computation of the spectral density magnitude of each captured pulse, our method exhibits better γ/n separation than the traditional charge-comparison method (CCM) with pulse-shape discrimination (PSD). Our method also outperforms other methods based on frequency-domain analysis in terms of classification performance for both CLYC and liquid scintillators. These advantages, combined with the ability to use the full detector energy range, make our proposal a good alternative to CCM with PSD for CLYC crystals coupled with SiPM arrays. Moreover, our method was devised for efficient implementation in real-time embedded applications based on Field-Programmable Gate Arrays (FPGA) or Digital Signal Processors (DSP).

* Corresponding author at: Dipartimento di Ingegneria e Architettura (DIA), Università degli Studi di Trieste (UNITS), Piazzale Europa, 1, Trieste, 34127, TS, Italy.

E-mail addresses: ivanrene.moralesargueta@phd.units.it, imorales@ictp.it (I.R. Morales).

https://doi.org/10.1016/j.net.2023.11.013

Received 3 July 2023; Received in revised form 26 September 2023; Accepted 7 November 2023

A tagged dataset of γ and n events was created as a sub-product of the data analysis performed to demonstrate the features of our method. This dataset includes raw pulse traces sampled at 100 MHz with an amplitude resolution of 10 bits. The calibrated energy in gamma-equivalent units and the proposed γ/n classification index are also provided for each event in the dataset.

2. Related work

Safari et al. [19] proposed a method based on frequency-domain analysis for pulse identification in mixed-gamma/neutron radiation environments. The experimental setup consisted of a cylindrical (D = 3", h = 3") BC501 liquid scintillator coupled to a fast PMT. Their main goal was to obtain a new classification metric based on a nonlinear weighting method. It was also demonstrated that a special case of the Discrete Fourier Transform (DFT) defines a new PSD parameter used in their method, described by a piecewise function that includes the zero-frequency (DC) component. The dataset was recorded at 5 GHz with an 8-bit amplitude resolution. They set a lower energy boundary to evaluate the figure-of-merit (FoM), discarding low-energy events. Their FoM, as defined in Section 6.2, was computed using only events higher than 200 keVee (kiloelectronvolt energy-equivalent) and was reported to be $(1.48 \pm 1.28 \times 10^{-2})$.

Dutta et al. [3] proposed analyzing the pulse decay times and the energy spectral density (ESD) of long trace windows that span through multiple events, recorded from a CLYC-based detector at 250 MHz with 12-bits resolution ADC. Their method aims at distinguishing gamma and neutron events in high-count-rate scenarios with a fast photomultiplier tube (PMT) coupled to the crystal. Pulse alignment is mandatory to achieve a precise pulse-decay time estimation. By using Parseval's theorem, they demonstrated how the ESD analysis (computed with DFT) correlates with the deposited energy of gamma or neutron (equivalent) events in the crystal. Their method uses a pulse-detector algorithm that executes an offline search for each recorded long trace (sample-by-sample) after a low-pass FIR filter is applied. The best FoM value at the lowest measured event rate was 1.35.

Nakhosti [20] used a similar detector setup as Safari et al. in [19]: a fast PMT coupled to a 2" BC501 A liquid scintillator. The author carried out an individual pulse analysis of triggered traces recorded at 4 GHz, aiming at considerably reducing the required sampling rate while still providing an acceptable FoM for gamma/neutron classification. The proposed method is based on the Fast Fourier Transform (FFT), in which the individual pulse shape information containing the features is preserved for signals recorded from liquid scintillators. After subsampling the raw data from 4 GHz down to 32 MHz, two energy cuts were analyzed individually: the first one for events between 50 keVee and 200 keVee, while the other accounted for the remaining pulses with energies higher than 200 keVee. The FoMs for the energy ranges were (0.62 ± 0.06) and (1.31 ± 0.04), respectively.

Polack et al. [21] stated that dealing with gamma/neutron classification with energies lower than 1 MeV is challenging. In addition, all the authors in [3,19,20,22,23] applied energy cuts to disregard low-energy events when computing the FoM, even with different types of scintillators (liquid, plastic, and CLYC) and light sensors (PMT and SiPM). Consequently, performing classification in the full detector energy range is still an issue to overcome.

3. Contributions

Based on existing developments and methods for γ/n classification using frequency-related analysis as well as the current requirements in the field with SiPM detectors, our contributions are described as follows:

- An improved classification FoM compared to PSD with CCM for SiPM-based CLYC detectors, featuring a less complex setup with superior immunity to strong magnetic fields.
- A method for gamma/neutron classification in the full detector energy range: from the thermal neutron region and tested up to 4.5 MeV fast neutrons without time-of-flight (ToF) calibration.
- A gamma/neutron classification method with a straightforward deployment capability to a real-time hardware platform using FPGA or DSP targets, taking advantage of the proven city-block-like simplification for approximate spectral density magnitude computation.
- The creation of a classified dataset of gamma/neutron mixed radiation events using an integrated SiPM-based CLYC detector as an added value to the existent PMT-based CLYC datasets. The resulting data were sampled at a sufficiently low rate, which is suitable for real-time applications targeting embedded systems. The dataset has been made publicly available at a data sharing platform.

4. Materials and methods

The development of our gamma/neutron classification method for a SiPM detector coupled with a CLYC (Cs2LiYCl6:Ce) crystal relies on experimental data. The detector, experimental setup, and data analysis used to validate the proposed method are described next.

4.1. SiPM-coupled integrated CLYC detector

The detector system is based on an off-the-shelf device manufactured by Scionix B.V., model V12.7B30/SIP-E3-CLYC-X. The small CLYC crystal with dimensions (D = 1/2", h = 1") is optically coupled to an OnSemi 2 × 2 SiPM array model ArrayC-60035-4P. A temperature-compensated bias power supply is integrated within the detector casing, along with a 50 Ω-coupled input and output preamplifier [24]. This setup allows for easy deployment without any external circuitry for a bias power supply, temperature compensation, or impedance matching, rendering it a good alternative for volume-constrained applications.

The crystal is sensitive to n_{th} events through the $[n + {}^{6}\mathrm{Li} \rightarrow T + \alpha$ (Q = 4.78 MeV)] neutron capture reaction, producing scintillation in the Ce^{3+} ions. The Q-value (Q) represents the energy released during the nuclear reaction and further manifests in the released tritium (T) and α particles. In the other hand, gamma photons interact by direct electron–hole capture by creating trapped hole centers, and by core-to-valence luminescence (CVL) [25]. The CVL process is responsible for the differences in the rise and fall times of γ and n events in the produced light, enabling the γ/n classification capabilities of the crystal [26]. The detection and spectroscopy of n_f was further reported [12], and is mostly caused by the $[n + {}^{35}\mathrm{Cl} \rightarrow {}^{35}\mathrm{S} + p$ (Q = 616 keV)] reaction, with a linear energy response up to 13 MeV [25]. These features render the CLYC crystal a viable alternative to n_{th} detectors based on He-3 [4] with an added value of n_f spectroscopy.

Neutron interactions within the crystal provoke scintillation events with a Q-value inherent to the reaction, observed as pulses on the γ energy-equivalent scale (keVee or MeVee). Quenching also occurs when the α and p (charged particles) products of the n_{th} and n_f events travel through the crystalline network, being this effect more significant for heavier particles [25]. Thus, the α particles generated by n_{th} capture in the ^{6}Li will suffer a larger degradation in the total energy deposition observed as the scintillation light, compared to that of the protons caused by the n_f reaction [10]. The indirect effect of n_{th} detection yields scintillation photons with an energy-equivalent magnitude of the Q-value (4.78 MeV) of the reaction multiplied by the 0.67 quenching factor for α, leading to pulses around 3200 keVee in the spectrum. In the case of n_f, the events are detected as the incoming neutron energy plus the Q-value of the reaction proton (Q = 616 keV) multiplied by the quenching factor of 0.84 [27]. This mechanism also allows the computation of the minimum energy at which n_f can be detected as a product of scintillation, around 616 keV× 0.84 = 517 keVee.

Using the CLYC detector coupled to a SiPM provides advantages for applications where coexistence with strong magnetic fields is mandatory [17,28] and linearity comparable to NaI(Tl) crystals for both γ and n_f spectroscopy is required [29,30]. Moreover, the integrated bias supply and preamplifier within the casing allow for a lightweight, smaller [17] and less complex setup (compared to the PMT counterparts) capable for applications such as remote mixed radiation monitoring with unmanned aerial vehicles (UAV) [16] and space exploration dosimetry [18,23]. The drawback of such integration level is the effect of pulse-shape degradation caused by the SiPM inherent capacitance [29,31,32], requiring a study of the derivatives of the raw pulse traces to set the parameters for pulse-shape discrimination [23], as described in Section 4.3.

4.2. Experimental setup

The experiment to record the data used in this work was conducted at the Neutron Science Facility (NSF) of the Nuclear Science and Instrumentation Laboratory (NSIL), International Atomic Energy Agency (IAEA), in Seibersdorf, Austria [33]. The resulting datasets were sampled with the detector described in Section 4.1 under the conditions detailed next.

4.2.1. Detector settings

Taking advantage of the integrated preamplifier in the detector, no external signal conditioning was required at its output, which allowed us to directly match it with the digitizer's 50 Ω input impedance. The bias voltage of the SiPM array was set to 28.7 V, as reported in the manufacturer's calibration sheet. Since shaping and gain parameters are not configurable, the detector is expected to behave as detailed in the calibration report.

4.2.2. Mixed radiation sources

One gamma-only dataset and two mixed neutron and gamma datasets were recorded. The gamma source used is a Caesium-137 (Cs-137) with a registered activity of 0.25 μCi in June 2015. Deuterium–tritium (DT) and deuterium–deuterium (DD) were used as neutron generators.

The DD emits a pulsed beam of monochromatic neutrons of 2.45 MeV with an estimated 4π neutron flux in the range of 10^6 neutrons/s, whereas the DT generates pulses of monochromatic neutrons of 14.1 MeV at an average rate set to 1.12×10^8 neutrons/s. The scattered neutrons in the surrounding matter reduce their energy, causing a continuum in the neutron spectrum up to the peak energy. Moreover, neutron activation of the surrounding matter and shielding lead to gamma radiation in both cases, generating a mixed-radiation field [34].

The events were digitized from the CLYC detector using a CAEN DT5761 digitizer, sampling at 4 Gsps (giga samples per second) with 10 bits of amplitude resolution. A cross-level trigger was used to capture individual traces containing single events with a threshold set at four standard deviations of the baseline Gaussian noise. The CLYC detector described in Section 4.1 was used throughout the experiment, subject to a stable temperature of 21 °C.

4.2.3. Data curation

The data were subsampled from the original 4 Gsps sampling rate down to 100 Msps (mega samples per second), aiming at using a reasonable execution frequency for embedded real-time deployments [35–38].

Three datasets were originally used, each featuring specific conditions, as described below.

- Gamma dataset: 20,000 events recorded from a Caesium-137 (Cs-137) gamma source
- DD neutrons dataset: 20,000 events recorded in a mixed radiation environment with the DD generator
- DT neutrons dataset: 20,000 events recorded in a mixed radiation environment with the DT generator

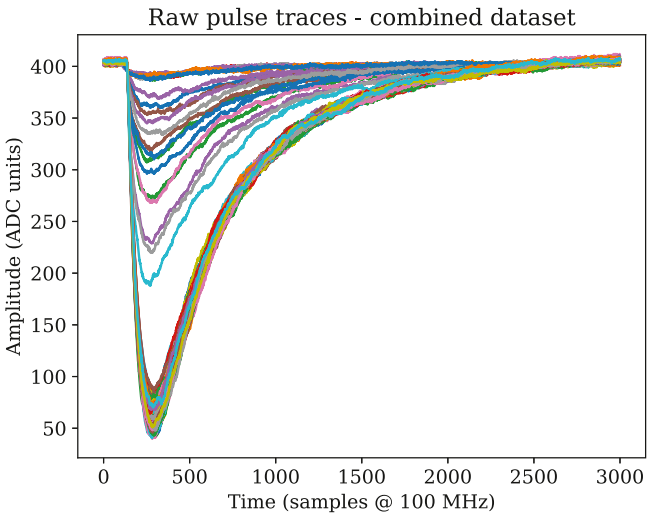

Fig. 1. Raw pulse traces after PU and saturated event removal, captured with a CLYC detector and downsampled to 100 Msps.

Table 1
Energy calibration points.

Source	Peak amplitude	Expected energy peak
Baseline	0.0 ADC bins	0.00 keVee
Cs-137 photopeak	74 ADC bins	662 keV
^{6}Li neutron capture	350 ADC bins	3160 keVee

The data were processed using the Pandas Framework version 1.5.2 and the NumPy numerical library version 1.23.5, running over Python version 3.10. Pile-up (PU) events and saturated traces were further removed as described in [39]. This process yielded three datasets containing the most representative pulse shapes under diverse experimental conditions.

Subsequently, after filtering out the undesired events, a joint dataset was created by adding the recorded traces from the gamma events to all the mixed neutron+gamma data (DD and DT). Hereafter, this dataset is referred to as DDTg, or simply the combined dataset, which is the basis of our study. Because the maximum energy range of our detector is about 4.5 MeVee, only fast neutrons and gamma pulses up to that limit are included. The energy for each event was estimated as the peak amplitude of the trace, referenced to the baseline average over 20 samples. Fig. 1 shows a subset containing some captured pulse shapes.

4.2.4. Energy calibration

Evidence exists on the linearity of detectors with a CLYC crystal coupled to a SiPM (based on SensL J-60035 arrays) when sensing events of up to 8 MeVee [23,29]. Consequently, calibration was carried out using only three points (including the baseline), as shown in Table 1. Fig. 2 shows the obtained linear regression curve, yielding a determination coefficient $r^2 = 0.999998$ and the equation defined as: $E = (9.024 \pm 0.015)x + (-2.54 \pm 3.29)$ [keVee], where x is the pulse peak amplitude in ADC units. The 3160 keVee neutron capture reaction peak was set according to the manufacturer's calibration report for the detector used in the experiment.

Both the Cs-137 gamma and ^{6}Li neutron capture reaction calibration peaks (in ADC units) were obtained using Gaussian distribution regressions of the energy histogram. The full-width at half-maximum (FWHM) energy resolutions were 8% and 7%, respectively.

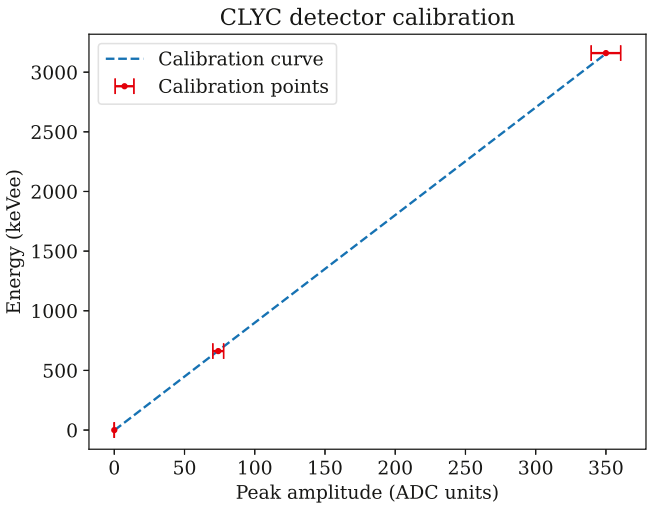

Fig. 2. Energy calibration curve of the CLYC detector with three reference points: baseline (0 keVee), Cs-137 photopeak (662 keV), and thermal neutron peak (3160 keVee).

4.3. Pulse-shape discrimination

The pulse-shape discrimination (PSD) index was computed with the CCM, similar to [40,41] and was used only as a reference for the traditional techniques applied to our detection system. The baseline was removed for each trace and the pulses were inverted on the x-axis to make them positive. Horizontal alignment was also performed using constant fraction discrimination (CFD) to ensure precise charge estimation for the CCM [42].

The intrinsic capacitance of the SiPM acts as an integrator, deforming the original pulse shape of the crystal response. By comparing the pulse decay times of a standard CLYC crystal coupled to a fast PMT [11] with our detector output in Fig. 3a (about 5 μs), it is apparent that some shaping is carried out in our case [23], presumably by the contribution of the SiPM capacitance and of the built-in preamplifier. To deal with the pulse shape deformation without requiring external hardware or pulse shape pre-processing during classification, a single gamma trace and neutron event were selected to further analyze the key points in their discrete derivatives. As usual [8,28,43], two discrete integration window ranges were defined to compute the PSD factor: short or prompt (W_s) and long or delayed (W_l). The short and long areas of each pulse in these ranges are computed as $A_s = \sum_{W_s} x_n$ and $A_l = \sum_{W_l} x_n$, being x_n each discrete value of the pulse under analysis. The PSD factor is computed as a ratio of the difference of the areas, as shown in Eq. (1):

$$PSD = \frac{A_l - A_s}{A_l} \tag{1}$$

The limits of such integration windows, expressed in sampling periods, were chosen according to the derivative plots shown in Fig. 3b, featuring the inflection points and slope values of both types of pulses. The window ranges were initially set as [55–100] for W_s and [55–150] for W_l. The highest FoM was achieved using the window ranges W_s = [50–105] and W_l = [50–170], after iteratively tuning these limits. Details of how the FoM is computed are provided in Section 6.2.

The derivatives were used as a reference to set the window ranges, with the pulse-shape discrimination analysis directly applied to the aligned data without amplitude normalization, as shown in Fig. 3a. Also, the derivative amplitudes of the normalized events indicate higher abundance of low-frequency components in the neutron pulse shape, giving a hint to how frequency analysis may be beneficial for discrimination.

5. Fourier-based classification

Contrary to the DFT-based method presented by Safari et al. [19], we disregard the zero-frequency component, providing the proposed classification index with substantial immunity to the baseline offset. In addition, no lower-energy neutron data are discarded, allowing the inclusion of all the recorded events regardless of their energy. Moreover, our method does not require either any further time-of-flight (ToF) calibration (as carried out in [44]) to achieve γ/n separation, even at the lowest energy range of fast neutrons. We also use a more computationally efficient method to obtain the DFT magnitude based on the FFT, as detailed in Section 5.1. The limitation of using the FFT is the requirement of using a power of two number of samples [45]: in our work 2^{11} (2048) samples were used for each triggered event.

Similar to the goals exposed in the work of Dutta et al. [3], we use a CLYC crystal to perform γ/n event discrimination based on the features extracted from the frequency-domain representation, resulting into a binary classification. However, our method does not require pulse alignment and each individual event is analyzed at a time. The proposed Frequency Classification Index (FCI) is based on the partial spectral area (PSA) of the computed FFT for each detected pulse.

In this work, the data were elaborated using frequency transformation (FFT) carried out by the SciPy library version 1.10.1.

5.1. Partial spectral area

Partial spectral area (PSA) has been defined as the discrete sum of the spectral density magnitude (SDM) components of the DFT of a trace within a defined frequency range. Let a single pulse trace be described as a discrete signal x_n, which is further transformed into the frequency domain using FFT for the DFT computation. This operation results in a complex expression X_k containing the frequency and phase components of the signal [46], as described in Eq. (2):

$$X_k = \sum_{n=0}^{N-1} x_n e^{-\frac{2\pi i}{N} kn}, \quad k = 0, \ldots, N-1 \tag{2}$$

Differences in the rise and decay times of both event types can be observed in Fig. 3a, where the neutron events contribute to a higher SDM in the lower frequency components. Consequently, we expect to observe the same differences in the frequency domain plot in Fig. 4, where the SDM of the first 2048 samples of the raw pulses (as in Fig. 1) is shown. It is straightforward to infer that events with higher low-frequency SDM components are more likely to be related to neutron events. It is also worth noting that the differences between the two types of events are apparent within the first 100 discrete frequency components, providing a hint of the integration limits for PSA computation.

Aiming at reducing the computational complexity in an embedded target, the approximate SDM (ASDM) is proposed as the sum of the absolute values of the real and imaginary parts of the DFT, also known as the city-block (CB) approach [47]. Instead of using the original definition involving the computation of a square root and two products, the CB alternative provides similar magnitude results with fewer computational requirements [48]. The ASDM is used from now on to compute the area of the PSA.

5.2. Frequency classification index

The FCI is the proposed index used to determine the likelihood of an event being a gamma or neutron based on its PSA features. Following the same approach as in Section 4.3, the FCI is defined as the ratio of the integrated short and long windows of the ASDM. In this case, the integration comprises the PSA within two ranges: low-frequency components PSA_l and wide-frequency components PSA_w. The integration ranges were optimized as described in Section 4.3 to achieve the maximum FoM, leading to [1–25] for the low-frequency

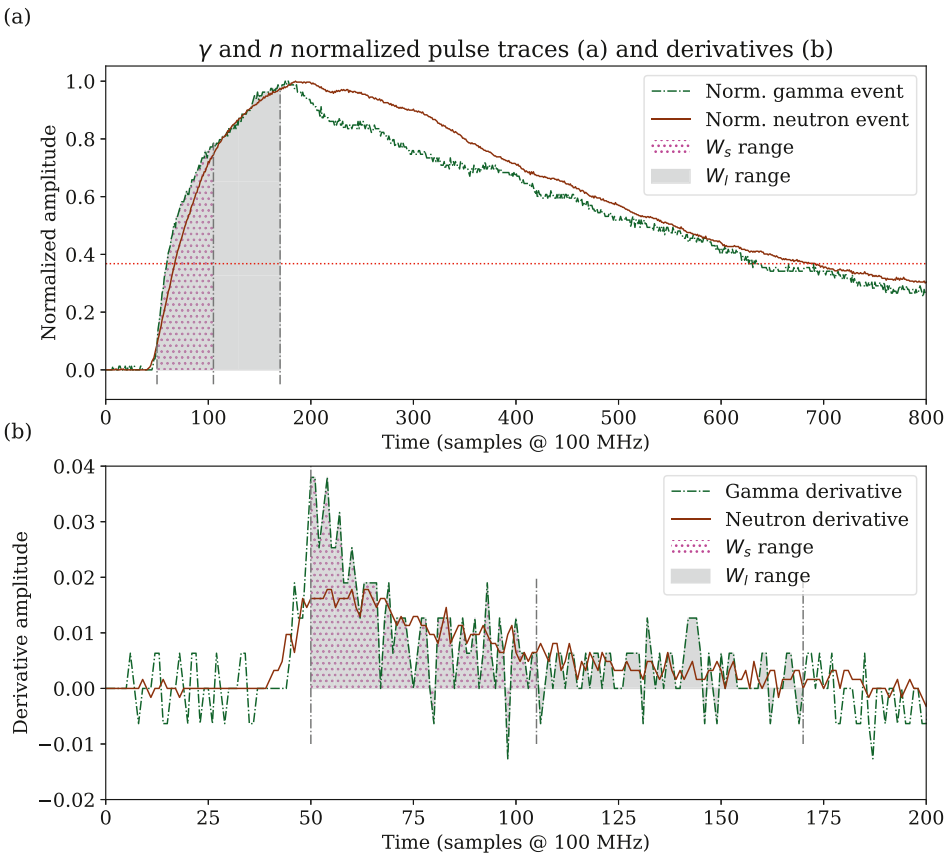

Fig. 3. (a) Normalized γ and n pulse traces with short (W_s) and long (W_l) integration windows for PSD. The horizontal line indicates the $(1/e)$-decay amplitude. (b) Trace derivatives of γ and n events with short and long integration windows. The integration limits for the PSD are W_s = [50–105] and W_l = [50–170].

integration window and [1–90] for the wide range in the discrete frequency axis, as highlighted in Fig. 4. It is worth mentioning that the zero-frequency component is not used to compute the FCI, providing the proposed method with immunity to baseline variations. Eq. (3) defines the FCI based on the described integration windows:

$$FCI = \frac{PSA_w - PSA_l}{PSA_w} \tag{3}$$

6. Results

The proposed γ/n classification method, based on frequency-domain analysis, has been evaluated using two quantitative criteria:

- The energy range on which the γ/n classification can be achieved with the proposed index FCI
- The classification performance compared to other methods based on frequency-domain analysis

The energy range and performance metrics are detailed in Sections 6.1 and 6.2, respectively.

In terms of the qualitative results, a two-class dataset with more than 38,000 gamma and neutron events was created and is publicly available at [49]. Each class contains not only the individual pulse traces sampled at 100 Msps, but also the calibrated energy and the FCI. Moreover, the possibility of making a precise implementation of the proposed method targeting embedded hardware deployments renders our solution an attractive alternative for applications that require real-time mixed-radiation event classification.

6.1. Neutron energy range

Because of CLYC's ^{35}Cl reaction with fast neutrons, the inherent Q-value and quenching losses create a scintillation energy equivalent to

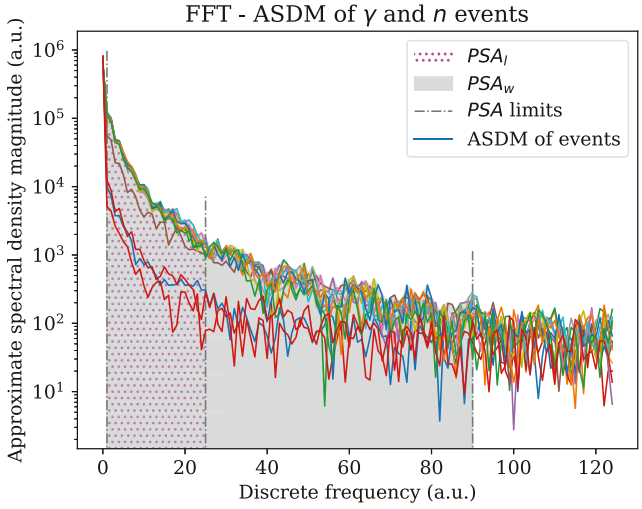

Fig. 4. Approximate spectral density magnitude (computed using FFT) of a set of pulses from the mixed γ/n dataset. The integration windows used to compute the FCI are delimited in the vertical dotted–dashed lines and marked as PSA_l and PSA_w, respectively. Events with higher ASDM in the PSA_l range are more likely to be related to neutrons.

517 keVee for the lowest-energy fast neutrons [25]. By applying this lower neutron energy-equivalent limit to the resolution of the detector (8%) in this energy range, the lowest detectable neutron energy is established to be about 476 keVee. Applying such an energy cut is mandatory in PSD with CCM to achieve an acceptable classification, leading to FoM = (1.11±0.02). However, our method based on frequency

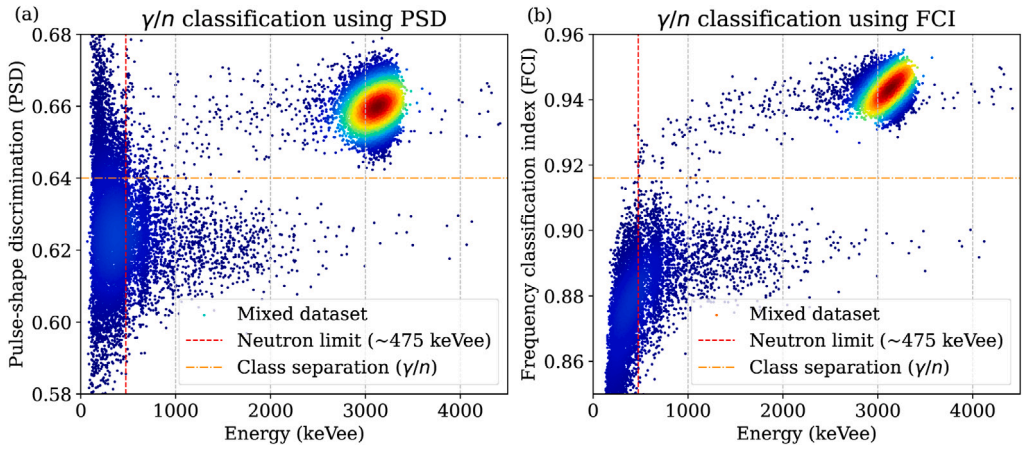

Fig. 5. Comparison of γ/n separation with PSD (a) and FCI (b). The neutron limit represents the lowest energy-equivalent value at which neutron events can be physically detected using a CLYC-based setup. The classification limit defines the discrimination between γ (lower cluster) and neutron (upper cluster) events. The FCI (b) qualitatively shows superior performance over the entire energy range. More evident is the comparison below the neutron detection energy limit, on which multiple γ events are misclassified using PSD, but an almost perfect classification is obtained with FCI.

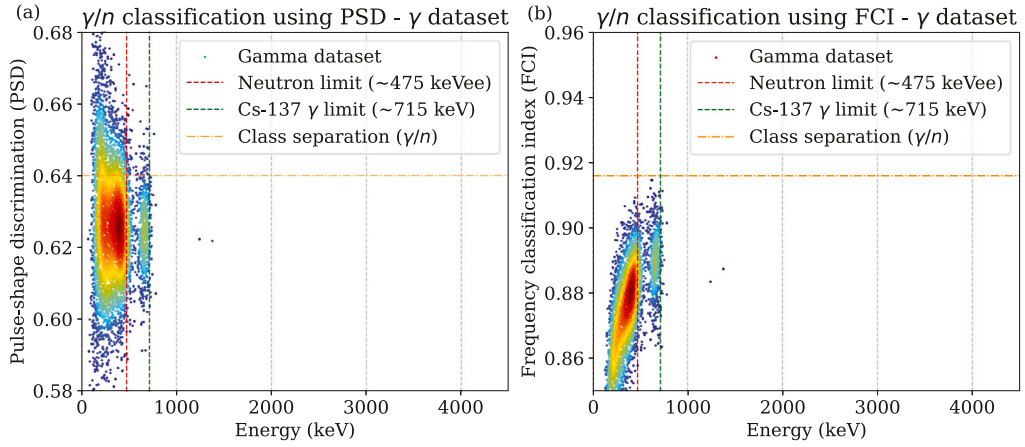

Fig. 6. The same axes as in Fig. 5 but with a Cs-137 γ-only dataset. Neutron-related events are meant to be clustered over the classification limit in both plots (a) and (b). The FCI method (b) shows a perfect classification for the events in the entire energy range, whereas the PSD with CCM (a) requires a lower energy cut to successfully separate both types of pulses. The maximum expected energy of the photons is marked as the Cs-137 limit in both plots, based on the known photopeak energy plus the detector FWHM resolution.

analysis does not require any energy cut, and γ/n classification is achieved automatically by a straight separation limit in the FCI. A detailed comparison of both methods is shown in Fig. 5, where the lower neutron energy limit depicts how well the FCI method distinguishes γ from n events, as expected from the physical behavior of the detector. Neutron interactions were grouped over the classification line, whereas gamma events remained below this limit.

As expected, thermal neutrons exhibit a dense cluster close to 3160 keVee because of the ^{6}Li neutron capture reaction in the crystal. Most of the remaining neutron events are caused by ^{35}Cl neutron scattering, providing not only counting capabilities, but also valuable spectroscopy information [25].

Fig. 6 reveals the actual classification power of the FCI method (Fig. 6b) compared to PSD with CCM (Fig. 6a), providing a better insight into how none of the events in the Cs-137 γ dataset have been misclassified as neutron events, even at the lowest energy.

6.2. Classification performance

We use the same FoM defined in [3,19–21] as the classification performance metric, as shown in Eq. (4). Variable S represents the distance between the gamma and neutron mean values of the distributions, whereas $FWHM_\gamma$ and $FWHM_n$ are the FWHM of each Gaussian curve for the γ and n events, respectively.

$$FoM = \frac{S}{FWHM_\gamma + FWHM_n} \tag{4}$$

To achieve equal comparison conditions, an energy cut was applied to the dataset for FoM estimation: events with energies below the neutron limit (approximately 475 keVee) were disregarded. This action does not affect the neutron detection capabilities with FCI though, since no neutron events are present below this energy limit within the gamma cluster, as shown in Figs. 5b and 6b.

The FoM was computed by integrating along the energy axis of both methods (PSD and FCI) down to the neutron energy limit, resulting in a histogram. The estimation of such a distribution is obtained from the sum of the two Gaussian functions. Fig. 7 shows the histograms and corresponding regressions performed to compute the FoM for both methods.

Superior classification is possible using the FCI (Fig. 7b) compared to the PSD with CCM (Fig. 7a) after evaluating our experimental data discrimination metrics. We also achieved the best FoM compared to other methods that use frequency domain analyses, accounting for the classification capabilities in the complete detector energy range. As a means of comparison with other implementations, another test was carried out to verify the performance of the FCI with an energy cut at 1 MeVee (the limit discussed in [21]), leading to a higher FoM. Table 2

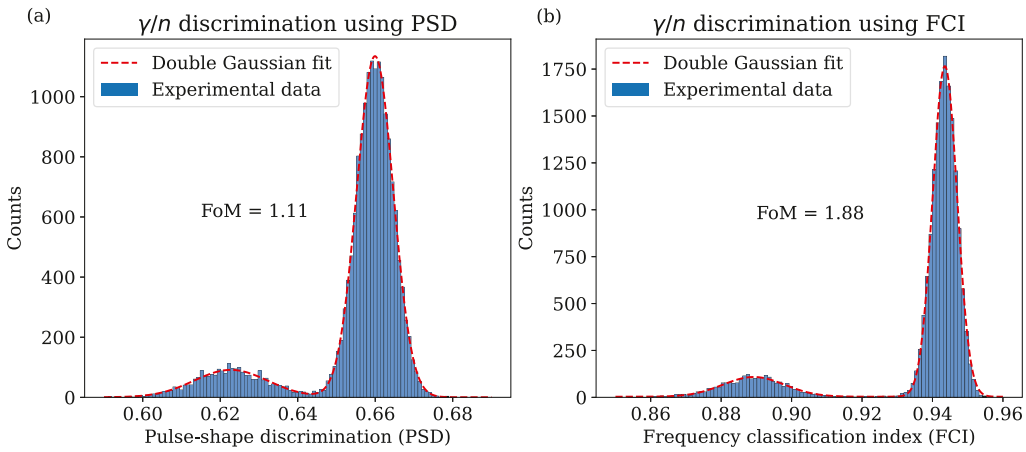

Fig. 7. FoM comparison of PSD (a) and FCI (b) for the same mixed γ/n dataset.

Table 2
Comparison of frequency-based methods for γ/n classification. The lowest energy range refers to the lowest neutron energy-equivalent limit on which classification from gamma events is possible in each study. ADC bins* units are used due to the absence of energy calibration in the referenced work. Our method was tested under two conditions: without any neutron being disregarded and with a low energy cut at 1 MeVee (the limit discussed in [21]).

Method	Best FoM	Lowest energy	Detection system
[3]	1.35	1930 ADC bins*	CLYC + PMT
[19]	1.48	200 keVee	BC501A + PMT
[20]	1.51	200 keVee	BC501A + PMT
Ours	1.88	No lower limit	CLYC + SiPM
Ours	2.13	1 MeVee	CLYC + SiPM

summarizes the results of our FCI and previous studies related to γ/n classification based on frequency analysis.

7. Discussion

Our method (FCI) achieved better classification performance (FoM) for gamma and neutron events when compared to other solutions based on frequency-domain analysis. We have also demonstrated a superior FoM for FCI compared to PSD with CCM when tested with the same experimental data. Moreover, reliable confirmation of the observed γ/n clusters with FCI is supported by the expected response of the CLYC crystal, even at the lowest n_f energy-equivalent range of the detector. No ToF calibration is required to achieve such results, demonstrating the CLYC capabilities as a standalone n_{th} detection and $n_f + \gamma$ spectroscopy system when coupled with SiPM sensors.

In contrast to other methods based on frequency-domain analysis for γ/n classification [3,20], our proposal was conceived for its deployment in embedded applications. The city-block simplification used in the approximate spectral density magnitude (ASDM) computation along with the 100 Msps sampling rate render our solution attractive for either FPGA or DSP real-time implementations.

A tagged dataset of gamma and neutrons was obtained after the data curation process. Such a dataset is valuable because of the low availability of classified γ/n traces sampled using a small integrated detector based on CLYC coupled to a SiPM array. It is worth mentioning that all analyzed traces were tagged, including pulses related to low-energy events. The dataset includes two types of events (classes): gamma photons and neutrons. The raw pulse traces and their corresponding calibrated energy are stored for each detected event up to 4.5 MeVee.

8. Future work

A hardware design to validate the proposed method using an embedded application is under development, targeting an AMD Artix-7 XC7A35T FPGA. The design prototype operates at 100 MHz with 10 bits amplitude resolution and computes the FFT with a transform length of 2048 samples, compatible with the data format presented in Section 4.2.3. Aiming at real-time operation, the system has been devised in a pipelined streaming scheme. The highest reported resource utilization in the FPGA is in the DSP blocks with a total of 37%, while the LUT and BRAM usage remain below 17% and 12%, respectively. Both the timing closure of the design (as reported by the development tool) and the resource utilization evidence the viability of implementing an embedded hardware solution to execute this γ/n classification method using a commercial FPGA device. The same design was also tested in an AMD Zynq 7z020 system-on-chip (SoC), reporting an overall resource utilization lower than 12%, suggesting the potential to exploit the parallelization capabilities in multiple detector systems.

Declaration of competing interest

The authors declare that they have no known competing financial interests or personal relationships that could have appeared to influence the work reported in this paper.

References

[1] R.T. Kouzes, A.T. Lintereur, E.R. Siciliano, Progress in alternative neutron detection to address the helium-3 shortage, Nucl. Instrum. Methods Phys. Res. A 784 (2015) 172–175, http://dx.doi.org/10.1016/j.nima.2014.10.046.

[2] J. Glodo, Y. Wang, R. Shawgo, C. Brecher, R.H. Hawrami, J. Tower, K.S. Shah, New developments in scintillators for security applications, Physics Procedia 90 (2017) 285–290, http://dx.doi.org/10.1016/j.phpro.2017.09.012.

[3] A. Dutta, P. Chandhran, K.E. Holbert, E.B. Johnson, Using decay time to discriminate neutron and gamma ray pulses from a CLYC detector, in: 2015 IEEE Nuclear Science Symposium and Medical Imaging Conference, NSS/MIC, IEEE, San Diego, California, USA, 2015, pp. 1–7, http://dx.doi.org/10.1109/NSSMIC.2015.7581902.

[4] A.M. Okowita, Characterization of Lithium-6 as a Commercial Helium-3 Alternative for Nuclear Safeguards and Security (Master's thesis), University of Tennessee - Knoxville, Knoxville, Tennessee, 2014, URL https://trace.tennessee.edu/utk_gradthes/3166.

[5] N. D'Olympia, P. Chowdhury, E. Jackson, C. Lister, Fast neutron response of 6Li-depleted CLYC detectors up to 20MeV, Nucl. Instrum. Methods Phys. Res. A 763 (2014) 433–441, http://dx.doi.org/10.1016/j.nima.2014.06.074.

[6] C.M. Whitney, L. Soundara-Pandian, E.B. Johnson, S. Vogel, B. Vinci, M. Squillante, J. Glodo, J.F. Christian, Gamma–neutron imaging system utilizing pulse shape discrimination with CLYC, Nucl. Instrum. Methods Phys. Res. A 784 (2015) 346–351, http://dx.doi.org/10.1016/j.nima.2014.09.022.

[7] F. Ferrulli, M. Labalme, M. Silari, Investigation of CLYC-6 for thermal neutron detection and CLYC-7 for fast neutron spectrometry, Nucl. Instrum. Methods Phys. Res. A 1029 (2022) 166460, http://dx.doi.org/10.1016/j.nima.2022.166460.

[8] B. Budden, L. Stonehill, N. Dallmann, M. Baginski, D. Best, M. Smith, S. Graham, C. Dathy, J. Frank, M. McClish, A Cs2LiYCl6:Ce-based advanced radiation monitoring device, Nucl. Instrum. Methods Phys. Res. A 784 (2015) 97–104, http://dx.doi.org/10.1016/j.nima.2014.11.051.

[9] M. Bourne, C. Mussi, E. Miller, S. Clarke, S. Pozzi, A. Gueorguiev, Characterization of the CLYC detector for neutron and photon detection, Nucl. Instrum. Methods Phys. Res. A 736 (2014) 124–127, http://dx.doi.org/10.1016/j.nima.2013.10.030.

[10] M. Smith, M. McClish, T. Achtzehn, H. Andrews, M. Baginski, D. Best, B. Budden, E. Clifford, N. Dallmann, C. Dathy, J. Frank, S. Graham, H. Ing, L. Stonehill, Assessment of photon detectors for a handheld gamma-ray and neutron spectrometer using Cs2LiYCl6:Ce (CLYC) scintillator, Nucl. Instrum. Methods Phys. Res. A 715 (2013) 92–97, http://dx.doi.org/10.1016/j.nima.2013.03.023.

[11] A. Giaz, L. Pellegri, F. Camera, N. Blasi, S. Brambilla, S. Ceruti, B. Million, S. Riboldi, C. Cazzaniga, G. Gorini, M. Nocente, A. Pietropaolo, M. Pillon, M. Rebai, M. Tardocchi, The CLYC-6 and CLYC-7 response to γ -rays, fast and thermal neutrons, Nucl. Instrum. Methods Phys. Res. A 810 (2016) 132–139, http://dx.doi.org/10.1016/j.nima.2015.11.119.

[12] M. Smith, T. Achtzehn, H. Andrews, E. Clifford, P. Forget, J. Glodo, R. Hawrami, H. Ing, P. O'Dougherty, K. Shah, U. Shirwadkar, L. Soundara-Pandian, J. Tower, Fast neutron measurements using Cs2LiYCl6:Ce (CLYC) scintillator, Nucl. Instrum. Methods Phys. Res. A 784 (2015) 162–167, http://dx.doi.org/10.1016/j.nima.2014.09.021.

[13] F. Pino, M. Polo, J.C. Delgado, G. Mantovani, S.M. Carturan, D. Fabris, D. Brunelli, L. Pancheri, A. Quaranta, S. Moretto, Evidence of fast neutron detection capability of the CLLB scintillation detector, Radiat. Phys. Chem. 202 (2023) 110494, http://dx.doi.org/10.1016/j.radphyschem.2022.110494.

[14] T. Huang, Q. Fu, S. Lin, B. Wang, NaI(Tl) scintillator read out with SiPM array for gamma spectrometer, Nucl. Instrum. Methods Phys. Res. A 851 (2017) 118–124, http://dx.doi.org/10.1016/j.nima.2017.01.068.

[15] D.D. Vita, L. Buonanno, F. Canclini, G. Ticchi, F. Camera, M. Carminati, C. Fiorini, A 144-SiPM 3" LaBr3 readout module for PMTs replacement in Gamma spectroscopy, Nucl. Instrum. Methods Phys. Res. A 1040 (2022) 167179, http://dx.doi.org/10.1016/j.nima.2022.167179.

[16] J. Hartman, A. Barzilov, I. Novikov, Remote sensing of neutron and gamma radiation using aerial unmanned autonomous system, in: 2015 IEEE Nuclear Science Symposium and Medical Imaging Conference, NSS/MIC, IEEE, San Diego, CA, USA, 2015, pp. 1–4, http://dx.doi.org/10.1109/NSSMIC.2015.7581763.

[17] O. Dendene, V.V. Afanasiev, S.V. Lushin, A.C. Chergui, A.A. Stifutkin, L. Boukerdja, Study of silicon photomultipliers (SiPM) with organic scintillator for neutron diagnostics of thermonuclear plasma, Fusion Eng. Des. 178 (2022) 113113, http://dx.doi.org/10.1016/j.fusengdes.2022.113113.

[18] J. Köhler, B. Ehresmann, C. Zeitlin, R. Wimmer-Schweingruber, D. Hassler, G. Reitz, D. Brinza, J. Appel, S. Böttcher, E. Böhm, S. Burmeister, J. Guo, H. Lohf, C. Martin, A. Posner, S. Rafkin, Measurements of the neutron spectrum in transit to Mars on the Mars science laboratory, Life Sci. Space Res. 5 (2015) 6–12, http://dx.doi.org/10.1016/j.lssr.2015.03.001.

[19] M.J. Safari, F.A. Davani, H. Afarideh, S. Jamili, E. Bayat, Discrete Fourier transform method for discrimination of digital scintillation pulses in mixed neutron-Gamma fields, IEEE Trans. Nucl. Sci. 63 (2016) 325–332, http://dx.doi.org/10.1109/TNS.2016.2514400.

[20] M. Nakhostin, Digital discrimination of neutrons and gamma-rays in liquid scintillation detectors by using low sampling frequency ADCs, Nucl. Instrum. Methods Phys. Res. A 916 (2019) 66–70, http://dx.doi.org/10.1016/j.nima.2018.11.021.

[21] J. Polack, M. Flaska, A. Enqvist, C. Sosa, C. Lawrence, S. Pozzi, An algorithm for charge-integration, pulse-shape discrimination and estimation of neutron/photon misclassification in organic scintillators, Nucl. Instrum. Methods Phys. Res. A 795 (2015) 253–267, http://dx.doi.org/10.1016/j.nima.2015.05.048.

[22] O. McCormack, L. Giacomelli, G. Croci, A. Muraro, G. Gorini, G. Grosso, R. Pasqualotto, E.P. Cippo, M. Rebai, D. Rigamonti, M. Tardocchi, Characterization and operational stability of EJ276 plastic scintillator-based detector for neutron spectroscopy, J. Instrum. 16 (2021) P10002, http://dx.doi.org/10.1088/1748-0221/16/10/P10002.

[23] W. Zhou, T. Cui, Z. Zhang, Y. Yang, H. Yi, D. Hou, Measurement of wide energy range neutrons with a CLYC(Ce) scintillator, J. Instrum. 18 (2023) P02014, http://dx.doi.org/10.1088/1748-0221/18/02/P02014.

[24] Scionix Holland B.V., Thermal neutron detector V12.7B30/SIP-E3-CLYC-x datasheet - Scionix, 2017, URL https://scionix.nl/wp-content/uploads/2017/03/V12.7B30_SIP-E3-CLYC-X.pdf. (Accessed 19 May 2023).

[25] M.C. Recker, Enabling Mobile Neutron Detection Systems with CLYC (Ph.D. thesis), Air Force Institute of Technology, Wright-Patterson Air Force Base, Ohio, 2019.

[26] P.A. Rodnyi, Core–valence luminescence in scintillators, Radiat. Meas. 38 (2004) 343–352, http://dx.doi.org/10.1016/j.radmeas.2003.11.003.

[27] J. Glodo, U. Shirwadkar, R. Hawrami, T. Achtzehn, H.R. Andrews, E.T.H. Clifford, H. Ing, V.D. Kovaltchouk, M.B. Smith, K.S. Shah, Fast neutron detection with Cs2LiYCl6, IEEE Trans. Nucl. Sci. 60 (2013) 864–870, http://dx.doi.org/10.1109/TNS.2012.2227499.

[28] N. Dinar, D. Celeste, M. Silari, V. Varoli, A. Fazzi, Pulse shape discrimination of CLYC scintillator coupled with a large SiPM array, Nucl. Instrum. Methods Phys. Res. A 935 (2019) 35–39, http://dx.doi.org/10.1016/j.nima.2019.04.099.

[29] S. West, D. Beckman, D. Coupland, N. Dallmann, C. Hardgrove, K. Mesick, L. Stonehill, Compact readout of large CLYC scintillators with silicon photomultipler arrays, Nucl. Instrum. Methods Phys. Res. A 951 (2020) 162928, http://dx.doi.org/10.1016/j.nima.2019.162928.

[30] T. Huang, Z. Zhang, Characterization of 1-inch CLYC scintillator coupled with 8 × 8 SiPM array, Nucl. Instrum. Methods Phys. Res. A 999 (2021) 165225, http://dx.doi.org/10.1016/j.nima.2021.165225.

[31] M. Altayeb, M. Zennaro, E. Pietrosemoli, Tinyml Gamma radiation classifier, Nucl. Eng. Technol. 55 (2023) 443–451, http://dx.doi.org/10.1016/j.net.2022.09.032.

[32] B.S. Budden, A.J. Couture, L.C. Stonehill, A.V. Klimenko, J.R. Terry, J.O. Perry, Analysis of Cs2LiYCl6:Ce3+ (CLYC) waveforms as read out by solid state photomultipliers, in: 2012 IEEE Nuclear Science Symposium and Medical Imaging Conference Record, NSS/MIC, IEEE, Anaheim, California, USA, 2012, pp. 347–350, http://dx.doi.org/10.1109/NSSMIC.2012.6551123.

[33] Nuclear Science and Instrumentation Newsletter No. 3, February 2022, Nuclear Science and Instrumentation Newsletter, (no. 3) INTERNATIONAL ATOMIC ENERGY AGENCY, Vienna, 2022.

[34] G.F. Knoll, Radiation Detection and Measurement, John Wiley & Sons, 2010.

[35] L.G. Garcia, R.S. Molina, M.L. Crespo, S. Carrato, G. Ramponi, A. Cicuttin, I.R. Morales, H. Perez, Muon–electron pulse shape discrimination for water Cherenkov detectors based on FPGA/SoC, Electronics 10 (2021) 224, http://dx.doi.org/10.3390/electronics10030224.

[36] L.H. Arnaldi, D. Cazar, M. Audelo, I. Sidelnik, The new data acquisition system of the LAGO collaboration based on the redpitaya board, in: 2020 Argentine Conference on Electronics, CAE, IEEE, Buenos Aires, Argentina, 2020, pp. 87–92, http://dx.doi.org/10.1109/CAE48787.2020.9046374.

[37] S. Moretto, F.P. Andrades, J. Delgado, C. Fontana, D. Fabris, G. Nebbia, M. Turcato, D. Brunelli, L. Pancheri, A. Quaranta, UAV prototype for localization and identification of radioactive contamination and emitters, EPJ Web Conf. 253 (2021) 08001, http://dx.doi.org/10.1051/epjconf/202125308001.

[38] P. Dejdar, P. Munster, T. Horvath, High-speed data acquisition and signal processing using cost effective ARM + FPGA processors, in: 2019 42nd International Conference on Telecommunications and Signal Processing, TSP, IEEE, Budapest, Hungary, 2019, pp. 593–596, http://dx.doi.org/10.1109/TSP.2019.8769055.

[39] R.E. Wurtz, Consistent principles for particle ID from PSD systems, in: A. Burger, R.B. James, S.A. Payne (Eds.), Hard X-Ray, Gamma-Ray, and Neutron Detector Physics XXI, SPIE, San Diego, California, United States, 2019, p. 34, http://dx.doi.org/10.1117/12.2528898.

[40] H. Ye, L. Chen, X. Xu, G. Jin, Fast FPGA algorithm for neutron–gamma discrimination, Nucl. Instrum. Methods Phys. Res. A 1027 (2022) 166256, http://dx.doi.org/10.1016/j.nima.2021.166256.

[41] M.E. Hammad, H. Kasban, R.M. Fikry, M.I. Dessouky, O. Zahran, S.M.S. Elaraby, F.E.A. El-Samie, Digital pulse processing algorithm for neutron and gamma rays discrimination, Analog Integr. Circuits Signal Process. 101 (2019) 475–487, http://dx.doi.org/10.1007/s10470-019-01498-8.

[42] H. Kasani, S. Ashrafi, N. Ghal-Eh, H.R. Vega-Carrillo, Gamma-ray spectroscopy with anode pulses of NaI(Tl) detector using a low-cost digitizer system, Appl. Radiat. Isot. 176 (2021) 109854, http://dx.doi.org/10.1016/j.apradiso.2021.109854.

[43] S.-X. Liu, W. Zhang, Z.-H. Zhang, S. Lin, H.-R. Cao, C.-X. Song, J.-L. Zhao, G.-Q. Zhong, Performance of real-time neutron/gamma discrimination methods, Nucl. Sci. Tech. 34 (2023) 8, http://dx.doi.org/10.1007/s41365-022-01160-5.

[44] H. Bai, G. Zhang, Z. Xiong, Y. Li, D. Zhao, M. Su, Z. Mo, X. Wang, F. Gao, H. Zhang, Z. Zhang, J. Wen, A method to calibrate the n-γ discrimination property of scintillators in low energy region, Appl. Radiat. Isot. 167 (2021) 109447, http://dx.doi.org/10.1016/j.apradiso.2020.109447.

[45] E.O. Brigham, R.E. Morrow, The fast Fourier transform, IEEE Spectr. 4 (1967) 63–70, http://dx.doi.org/10.1109/MSPEC.1967.5217220.

[46] A.V. Oppenheim, A.S. Willsky, S.H. Nawab, Signals and Systems, Prentice Hall, London, 1997.

[47] T. Alharbi, Distance metrics for digital pulse-shape discrimination of scintillator detectors, Radiat. Phys. Chem. 156 (2019) 205–209, http://dx.doi.org/10.1016/j.radphyschem.2018.11.014.

[48] A. Cicuttin, I.R. Morales, M.L. Crespo, S. Carrato, L.G. García, R.S. Molina, B. Valinoti, J.F. Kamdem, A simplified correlation index for fast real-time pulse shape recognition, Sensors 22 (2022) 7697, http://dx.doi.org/10.3390/s22207697.

[49] I.R. Morales, Gamma and neutron tagged dataset from CLYC SiPM detector, 2023, http://dx.doi.org/10.5281/zenodo.8037058, URL https://zenodo.org/record/8037239. (Accessed 14 June 2023).